-RESEARCH PAPER-

International Journal of Mining and Geo-Engineering

IJMGE

IJMGE 60-3 (2026) 287-301

DOI: 10.22059/IJMGE.2026.413985.595371

Mixed-norm modeling of airborne tensor gravity and total field magnetic data to image the intrusion related gabbroic Budgell Harbour stock

Fatemeh Didar [a] , Mojtaba Hosseini [a] , Maysam Abedi [a, *] , Vahid Ebrahimzadeh Ardestani [b] and Zahra Sadat Mohammadi Saroughi [b]

[a] *School of Mining Engineering, College of Engineering, University of Tehran, Tehran, Iran.*

[b] *Institute of Geophysics, University of Tehran, Tehran, Iran.*

Article History:

Received: 07 May 2026.

Revised: 23 May 2026.

Accepted: 26 August 2026.

ABSTRACT

This study examines the subsurface architecture of a gabbroic body located in the Newfoundland region (Newfoundland and Labrador, Canada) by analyzing tensor gravity and total magnetic intensity data. The primary objective is to assess the effectiveness of various regularization strategies within a mixed-norm inversion framework for improving the reconstruction of the geometry and physical property distribution of the gabbroic body and its associated anomalous zones. To this end, following initial preprocessing, the gravity and magnetic datasets were inverted under three scenarios employing mixed ℓ_0, ℓ_1 and ℓ_2 norm configurations, respectively, thereby enabling a comparative evaluation of the influence of sparsity versus smoothness constraints on inversion outcomes. The results demonstrate that sparser norms are more effective at delineating compact, high-contrast anomalous bodies, while smoother norms yield superior recovery of continuous structural features and regional background trends. A comparative analysis of the two datasets reveals that magnetic data exhibit greater sensitivity to variations linked to magnetic mineralization within the gabbroic body whereas gravity data offer more robust constraints on the overall geometry and density distribution of the body. All inversion experiments achieved stable convergence, and the resulting models successfully delineated both the primary structure of the body and its associated anomalous zones. Collectively, the findings of this study indicate that employing a mixed-norm inversion framework jointly with gravity and magnetic data constitutes an effective approach for reducing ambiguity and enhancing the interpretation of subsurface structures in complex geological settings, such as gabbroic intrusions.

Keywords: *Mixed-norm, Gabbroic intrusion, Newfoundland, Gravity and magnetic, Inversion.*

1. Introduction

The gabbroic body represents one of the most important types of mafic intrusive igneous rocks and can be effectively characterized through integrated geological and geophysical investigations. These bodies, primarily composed of plagioclase, pyroxene, and occasionally olivine, represent magmatic processes occurring at depth within the Earth's crust. They provide valuable insights into magma sources, crystallization conditions, and crustal evolution. Geophysically, gabbros represent viable exploration targets for gravity, magnetic, and seismic methods, given their high density, high seismic velocities, and appreciable magnetic properties. In addition, the occurrence of gabbroic bodies may be associated with the concentration of economically important mineral deposits such as chromite, titanium, vanadium, nickel–copper sulfides, and platinum-group elements (PGE). Therefore, their identification and investigation are crucial not only for understanding crustal structure but also for mineral resource exploration [1-4]. Gabbroic bodies generally have a higher density than their host rocks and therefore produce positive gravity anomalies at local to regional scales. Due to the presence of minerals such as magnetite, ilmenite, titanomagnetite, and occasionally chromite, they are also sources of strong magnetic anomalies and elevated radiometric responses [5-9]. Due to the complex geometry and heterogeneity of these bodies, the use of advanced inversion methods is essential for interpreting potential field data.

Potential field methods, particularly gravity and magnetic surveys, are among the most commonly applied non-seismic techniques in geophysical exploration. They are typically carried out using both ground-based and airborne systems and are widely employed to investigate diverse geological environments, including mineralized zones and intrusive igneous complexes [10-14]. The objective of this study is to employ a smooth mixed-norm inversion approach on gravity and magnetic data to construct a three-dimensional model of a gabbroic body and to mitigate ambiguity in the interpretation of subsurface structures. The smooth mixed-norm inversion method represents an advanced technique for geophysical data interpretation that, through the integration of soft constraints and prior information, facilitates the derivation of more realistic subsurface structural models. Unlike classical inversion approaches that depend primarily on data misfit minimization, this methodology concurrently incorporates geological knowledge, physical constraints, and structural interrelationships. This feature reduces the inherent non-uniqueness of the inverse problem, enhances solution stability, and improves the resolution of the resulting model. The smooth mixed-norm approach is particularly valuable in complex scenarios characterized by noisy or incomplete data, as well as those admitting multiple feasible solutions. Consequently, it yields more reliable outcomes in the interpretation of gravity, magnetic, electrical resistivity, and seismic data. Thus, this method is widely recognized as

* Corresponding author: *E-mail address:* maysamabedi@ut.ac.ir (M. Abedi).

an effective tool for characterizing geological structures and mitigating uncertainty in exploration geophysics [15-19].

In geophysical inversion problems, classical ℓ_2 (Tikhonov) norms, and later ℓ_1 norms, have been used for decades to control model smoothness or sparsity. However, these approaches impose a single type of behavior—either purely smooth or purely sparse—across the entire model domain, which is insufficient for representing complex geological structures [15, 16]. To overcome this limitation, the use of ℓ_{pq} norms with $(0 < p \text{ or } q < 2)$, and in particular mixed-norm formulations in the regularization term, has been proposed. The goal is to obtain models that are "compact with sharp boundaries" in some regions of the model space and "smooth" in others [15, 16, 21]. Among the earliest structured contributions in this area is the work of Fournier and Oldenburg, who introduced the concept of mixed ℓ_p-norm inversion. Their framework enables the application of different norms to the model and its gradients, and even allows the parameter (p and q) to vary across different subdomains [17]. They employed Lawson's formulation and the Iteratively Reweighted Least Squares (IRLS) method, along with its scaled variant (S-IRLS), to solve this nonlinear problem [17-19]. In summary, the key pioneers in the direct application of mixed ℓ_p-norm regularization in geophysical inversion can be primarily traced to the work of Fournier and Oldenburg on gravity and magnetic inversion [17-19], followed by subsequent developments on sparse potential field inversion and uncertainty analysis [17, 18, 22].

Within the Budgell Harbour Stock (BHS) gabbroic body in north-central Newfoundland, studies of magnetic and tensor gravity data have been primarily conducted by the Peace et al. [23]. In a comprehensive petrophysical study, they integrated airborne full tensor gravity (FTG) data, airborne magnetic data, and structural observations to model the irregular geometry, southward dip, and lobate magma conduits associated with lamprophyre dykes surrounding the BHS. Their work also investigated the role of these features in magmatism related to the opening of the North Atlantic Ocean [20]. Subsequently, Geng et al. conducted several studies in which they first performed probabilistic three-dimensional inversion of airborne FTG data for the BHS [21, 22]. They then applied joint three-dimensional inversion of airborne FTG and magnetic data to recover the distribution of density and magnetic susceptibility, leading to improved delineation of the main intrusive body and the shallow dyke systems [23, 24]. The structural data and the three-dimensional density and magnetic susceptibility models derived from these inversions were subsequently published as an independent dataset. These results now constitute the primary reference for geophysical and structural information on the BHS and the Notre Dame Bay region [15].

Geophysical modeling in this study was conducted using the open-source SimPEG library (version 0.25.2), which offers a robust framework for parameter estimation [28]. The inversion modeling was performed on an ASUS laptop equipped with an Intel® Core™ i7-13620H processor (2.4 GHz base frequency) and 32 GB of RAM.

2. Methodology

In this section, we first present the mathematical formulation of gravity and magnetic forward modeling. Subsequently, we provide a detailed analysis of the mixed-norm inversion approach applied to the independent inversion of gravity and magnetic data.

2.1. Forward modelling

Solving the forward problem allows us to predict geophysical datasets that correspond to particular subsurface geological structures. In essence, through the utilization of model parameters (**c**) as an example, we can predict the resultant data (**d**), utilizing A_s as the mathematical operator for forward modelling connected to the causative source $\boldsymbol{s}$ [25]:

$$\boldsymbol{d} = A_s(\boldsymbol{c}) \tag{1}$$

For gravity-gradient forward modelling, the vertical gravity gradient component (g_{zz}) was employed. The observed response is linked to the subsurface density distribution through the sensitivity kernel T_{zz}, which transforms the density contrast of each discretized cell (ρ) into the predicted gravity-gradient response at observation point P (x_P, y_P, z_P) [26].

$$\boldsymbol{g} = \begin{bmatrix} T_{xx} \\ T_{xy} \\ T_{xz} \\ T_{yy} \\ T_{yz} \\ T_{zz} \end{bmatrix} \rho \,. \tag{2}$$

The vertical gravity-gradient component (g_{zz}) is selected from the full gravity tensor dataset due to its superior sensitivity to near-surface density variations and its higher spatial resolution compared with the other tensor components. Among all full tensor components, (g_{zz}) provides the most stable and interpretable response for delineating compact and high-contrast subsurface structures. For this reason, it is particularly well suited for the inversion framework adopted in this study. The corresponding forward response is described by Eq. (3).

$$g_{zz} = T_{zz}\rho \,. \tag{3}$$

The specification of T_{zz} is outlined in Eq. (4) [27]:

$$T_{zz} = G\left(arctan\left(\frac{d_x d_y}{r d_z}\right) - \frac{d_x d_z}{r(d_y + r)} - \frac{d_y d_z}{r(d_x + r)}\right)\Big|_{x_L}^{x_U}\Big|_{y_L}^{y_U}\Big|_{z_L}^{z_U} \tag{4}$$

$$r = \left(d_x^2 + d_y^2 + d_z^2\right)$$

$$dx = \left(x_p - x\right), dy = \left(y_p - y\right), dz = \left(z_p - z\right).$$

In each unit cell, the relative distance components (d_x, d_y, d_z) between the observation point and the prism boundaries are defined using the coordinates of the lower southwest corner $L(x_L, y_L, z_L)$ and the upper northeast corner $U(x_U, y_U, z_U)$. The Euclidean distance is given by $r = \sqrt{(d_x{}^2 + d_y{}^2 + d_z{}^2)}$ which is used in the formulation of the gravity-gradient sensitivity kernels. In gravity-gradient forward modelling, the response is governed by second-order spatial derivatives of the gravitational potential, which makes the formulation more sensitive to small-scale density variations compared to conventional gravity (g_z). For a large number of observation points, the forward problem is expressed in matrix form as given in Eq. (5) [18].

$$\boldsymbol{g}^{pre} = \mathbf{F}_{\boldsymbol{G}}\rho \tag{5}$$

In the equation provided, $\mathbf{F}_{\boldsymbol{G}}$ represents the linear forward operator matrix used in gravity modelling. It transforms the space of physical parameters into the data space denoted as $\boldsymbol{g}^{pre}$, where $\rho \in R^{\mathrm{M}}$, $\boldsymbol{g}^{pre} \in R^{\mathrm{N}}$, $\mathbf{F}_{\boldsymbol{G}} \in R^{\mathrm{N}\times\mathrm{M}}$. Here, M signifies the total number of cells, and N indicates the number of observation points [18, 27].

For magnetic forward modelling [19, 28], we start by defining the forward problem analogous to Eq. (2). This linear system is expressed in Eq. (6), where **S** represents a symmetric matrix that describes the linear relationship between a prism with magnetization $\mathbf{m}^*=[M_x, M_y, M_y]^S$ and the magnetic field components $\mathbf{b}=[b_x, b_y, b_z]^S$.

$$\mathbf{b} = \mathbf{S}\mathbf{m}^* \tag{6}$$

The tensor **S**, detailed in Eq. (7), is a symmetric matrix with a zero trace. Its components are $S_{xx}, S_{xy}, S_{xz}, S_{yy}, S_{zy}, S_{zz}$.

$$\mathbf{S} = \frac{\mu_0}{4\pi}\begin{bmatrix} S_{xx} & S_{xy} & S_{xz} \\ S_{xy} & S_{yy} & S_{zy} \\ S_{xz} & S_{yz} & S_{zz} \end{bmatrix} \tag{7}$$

Finally, we can formulate the total field magnetic intensity (TMI) forward modelling equation analogous to Eq. (5), as shown in Eq. (8). Here, $\mathbf{F}_{\boldsymbol{T}}$ is the forward operator matrix for magnetic modelling, with $\mathbf{m}^* \in R^{3\mathrm{M}}$, $\mathbf{b}^{pre} \in R^{\mathrm{N}}$, $\mathbf{F}_{\boldsymbol{T}} \in R^{\mathrm{N}\times 3\mathrm{M}}$ [19, 28].

$$\mathbf{b}^{pre} = \mathbf{F}_{\boldsymbol{T}}\mathbf{m}^* \tag{8}$$

2.2. Inverse modelling

The theoretical foundation for the inversion methodology employed within the SimPEG framework is laid out in the pioneering works of Li and Oldenberg (1996, 1998) [29, 30]. Subsequently, Fournier et al. (2016, 2019) introduced a more advanced and robust framework for this approach [17, 19]. This inversion method is typically based on minimizing an objective function, which is classified as an optimization problem and formulated as follows:

$$min\ \phi(m) = \phi_d + \beta\phi_m\ . \tag{9}$$

In Eq. (9), $\phi(m)$ denotes the objective function to be minimized through the iterative inversion process. The component ϕ_d represents the data misfit term, ensuring that the recovered model accurately predicts the field observations (gravity and magnetic data). The component ϕ_m is the model objective function or regularization function, which ensures the recovered model reflects plausible geological features and exploration targets. Lastly, the parameter β balances the relative contributions of ϕ_d and ϕ_m within the final objective function $\phi(m)$ [29, 30]. The misfit function expressed in Eq. (10) quantifies the disparity between observed data ($\boldsymbol{d}^{obs}$) and predicted data ($\boldsymbol{d}^{pred}$) and $\boldsymbol{\sigma}$ represents the estimated uncertainties in the data [29-31].

$$\phi_d = \sum_{i=1}^{N}\left(\frac{\boldsymbol{d}_i^{pred} - \boldsymbol{d}_i^{obs}}{\boldsymbol{\sigma}_i}\right)^2 \tag{10}$$

The regularization function (ϕ_m) introduces prior information and constraints to the inverse problem, mitigating its inherent non-uniqueness. The most frequently used approach employs the L_2-norm measure, leading to a discrete linear system as shown in Eq. (11):

$$\phi_m = \alpha_s\phi_s + \alpha_x\phi_x + \alpha_y\phi_y + \alpha_z\phi_z = \sum_{r=s,x,y,z}\alpha_r\ \|\mathbf{W}_r\mathbf{V}_r\mathbf{G}_r(\mathbf{m}-\mathbf{m}^{ref})\|_2^2 \tag{11}$$

In Eq. (11), the term ϕ_s measures the deviation of the discrete model ($\mathbf{m}$) from a reference model ($\mathbf{m}^{ref}$). The reference model m^{ref} is defined over the active cells of the computational mesh, which correspond to the subsurface region below the topography and are selected using an identity mapping. For the gravity inversion, the reference model is defined as a zero-valued homogeneous background, and the initial model is also set to zero. This implies that density variations are reconstructed as perturbations relative to a null reference medium. For the magnetic inversion, a constant value of 1×10^{-5} is assigned uniformly to all active cells as the background susceptibility model, allowing magnetic susceptibility contrasts to be recovered relative to a homogeneous medium. This configuration provides a consistent anomaly-based inversion framework for both datasets in the absence of detailed a priori geological information. The resulting homogeneous model provides a neutral starting point from which deviations are recovered during inversion. ϕ_x, ϕ_y, and ϕ_z assess the roughness of the model in the respective x, y, and z directions. The coefficients α_s, α_x, α_y, and α_z regulate the closeness of the derived model to the reference model and control the smoothness of the resulting model, respectively [29-31]. The matrices $\mathbf{G}_x$, $\mathbf{G}_y$, and $\mathbf{G}_z$ represent discrete gradient operators, which are used to calculate the model gradients in different directions [29, 30]. For the smallness component, $\mathbf{G}_s$ reduces to the identity matrix, indicating that it does not contribute to the gradient computation. The term $\mathbf{W}_s$ represents the weight associated with the smallest model component, ensuring that the smallest possible model is favored. Similarly, $\mathbf{W}_x$, $\mathbf{W}_y$ and $\mathbf{W}_z$ are weights that correspond to the flatness of the model in the x, y, and z directions, promoting smooth transitions in the model across these axes. The matrix $\mathbf{W}_m$ represents the combined weighting matrix that integrates all of the aforementioned weights, thereby providing a balanced framework for enforcing both model fidelity to the reference and smoothness across all dimensions. This comprehensive weighting scheme ensures that the resulting model is both physically plausible and spatially smooth, while adhering to the imposed constraints and available prior information [29-31].

Under the mixed-norm ℓ_{pq} framework [17, 19, 32, 33], the regularization term can be expressed as follows, where $(0 \le p, q \le 2)$ [19]. The mixed-norm approach allows for the generation of more accurate deposit models and enables the application of different norms to various components of the regularization term. Models with $p = 0$ (or q) exhibit superior performance in recovering the target body and produce sharper boundaries. Models with $p = 2$ perform less effectively in target recovery and yield smoother, more diffuse models, while models with $p = 1$ demonstrate intermediate behavior. Exact ℓ_0 norm minimization is a non-convex and NP-hard optimization problem and is therefore computationally infeasible for practical geophysical inversion problems. In this study, sparsity promotion is achieved through an Iterative Reweighted Least Squares (IRLS) strategy, which replaces the original problem with a sequence of weighted least-squares approximations. In this framework, the weighting coefficients are adaptively updated at each iteration based on the evolving model estimate, gradually enhancing sparsity in the recovered solution. This procedure does not correspond to an exact ℓ_0 formulation, but rather to a surrogate sparsity-inducing approximation that emulates its behavior in a computationally efficient manner. The iterative process is terminated when changes in the model parameters and data misfit fall below predefined thresholds or when a maximum number of iterations is reached.

$$\phi_m^{pq} = \alpha_s\|\mathbf{W_s}\mathbf{V_s}\mathbf{R_s}(\mathbf{m})\|^p + \sum_{r=x,y,z}\alpha_r\|\mathbf{W_r}\mathbf{V_r}\mathbf{R_r}\mathbf{D}_r(\mathbf{m})\|^q \tag{12}$$

where $\mathbf{G}_r$ is substituted with the finite difference operator $\mathbf{D}_r$ as represented below[18, 19]:

$$\mathbf{D}_r = \begin{bmatrix} -1 & 1 & 0 & \cdots & 0 \\ 0 & \ddots & \ddots & \ddots & \vdots \\ \vdots & \cdots & 0 & -1 & 1 \end{bmatrix} \tag{13}$$

We utilize a scaled iterative reweighted least squares method (S-IRLS) to tackle a sequence of weighted least squares problems iteratively. The computation of the IRLS weight ($\mathbf{R}_r$) is outlined below [18, 19]:

$$\mathbf{R}_r = diag\left[\left(\epsilon_r^2 + \left(\mathbf{D}_r\mathbf{m}^{(k-1)}\right)^2\right)^{\frac{p_r}{2}-1}\right]^{\frac{1}{2}} \tag{14}$$

In the provided equation, ϵ stands for the threshold parameter, $\mathbf{m}^{(k-1)}$ represents the model obtained from the preceding iteration, and $\mathbf{V}_r$ (Eqs. 11 and12) signifies the volume terms linked with the discretization. Additionally, p_r denotes the regularization parameter linked with the direction (e.g., x, y, or z). Through iterative updating of these weights, the IRLS method facilitates the convergence of the inversion process toward a solution that effectively balances the fit to the observed data and adheres to the regularization constraints [18]. The final objective function for the mixed-norm inversion of gravity and magnetic data is described as follows, where the symbol $\boldsymbol{\kappa}$ denotes the magnetic susceptibility and $\boldsymbol{\rho}$ represents the density contrast through the gravity inversion:

$$\min\phi(m)_{grav} = \|\left(\mathbf{F}_G\boldsymbol{\rho} - \mathbf{d}_{grav}{}^{obs}\right)\|_2^2 + \beta\left(\alpha_s\|\mathbf{V_s}\mathbf{R_s}\boldsymbol{\rho}\|^p + \sum_{r=x,y,z}\alpha_r\ \|\mathbf{V_r}\mathbf{R_r}\mathbf{D_r}\boldsymbol{\rho}\|^q\right)$$

$$\min\phi(m)_{mag} = \|\left(\mathbf{F}_b\boldsymbol{\kappa} - \mathbf{d}_{mag}{}^{obs}\right)\|_2^2 + \beta\left(\alpha_s\|\mathbf{V_s}\mathbf{R_s}\boldsymbol{\kappa}\|^p + \sum_{r=x,y,z}\alpha_r\ \|\mathbf{V_r}\mathbf{R_r}\mathbf{D_r}\boldsymbol{\kappa}\|^q\right) \tag{15}$$

In the inversion process, the weighting coefficients were assigned as $\alpha_s = \alpha_x = \alpha_y = \alpha_z = 1$, implying equal contributions of the smallness and smoothness constraints in all directions. The regularization parameter β was set to 1 for gravity inversion and 5 for magnetic inversion, based on empirical tests to obtain a stable balance between data misfit and model smoothness.

In this study, the inversion is performed using a projected Gauss–Newton conjugate gradient (GNCG) optimization scheme. Multiple stopping criteria are used to ensure stability and consistency of the recovered model. Specifically, the inversion is terminated when the data misfit reaches the expected noise level. Within the IRLS framework, convergence is additionally monitored through the relative change in

the objective function. The IRLS iterations are stopped when this change falls below a prescribed threshold (10^{-4}) or when a maximum of 30 iterations is reached, whichever occurs first. An overall maximum iteration limit is also enforced as a safeguard. These criteria collectively ensure a controlled inversion process, preventing overfitting while maintaining consistency with the assumed noise characteristics of the data.

3. Geological setting

Newfoundland Island constitutes the northern segment of the Appalachian orogenic belt. Its geological framework is subdivided into multiple tectonostratigraphic zones, delineated on the basis of variations in stratigraphy and structural attributes related to the evolution and subsequent breakup of a late Precambrian tectonic regime [34]. One of the principal tectonostratigraphic units is the Humber Zone, which comprises Paleozoic, shelf-derived sedimentary sequences deposited unconformably atop the crystalline Precambrian Grenville basement. This zone preserves evidence of multiple deformation phases that affected the Cambrian–Ordovician passive margin, along with the Ordovician to Devonian foreland basin systems, all of which were influenced by the Taconian, Salinian, and Acadian orogenic episodes [35]. The Dunnage Zone, encompassing the Budgell Harbour area, is defined by Ordovician ophiolitic suites and associated arc-related complexes formed in an oceanic setting external to the Laurentian margin. Its contact with the Humber Zone is marked by the Baie Verte Line, a major, protracted, and structurally composite fault system [40]. The Gander Zone consists largely of deep-marine sedimentary successions deposited along the eastern margin of the Paleozoic Ocean basin. To the southeast, it is tectonically juxtaposed against the Avalon Zone—a terrane of Gondwanan origin that records stratigraphic and structural signatures of ancient subduction processes [41]. The Avalon Zone comprises Early Paleozoic platformal sedimentary strata and Late Precambrian volcanic–plutonic assemblages, interpreted as continental fragments with European affinities [42].

Situated within the Dunnage Zone of north-central Newfoundland, the BHS represents a mafic intrusive complex composed predominantly of olivine gabbro, hornblende gabbro, biotite–hornblende peridotite, diorite, diatreme breccias, and lamprophyre dikes. The associated dike swarm displays a radial pattern centered upon the BHS, indicating that these structures propagated outward into the host country rocks during emplacement of the intrusive body and its related magmatic activity [23]. The BHS is interpreted as a distinctive alkaline ultramafic intrusive body, probably associated with a major regional fault system. This tectonic feature may have significantly influenced the development of offshore Newfoundland's sedimentary basins, which are currently of interest for hydrocarbon exploration [43]. Globally, the majority of platinum and palladium resources are found in laterally extensive, well-defined reef-like horizons, typically developed within layered igneous intrusions or at mafic–ultramafic contacts [43]. Because such geological environments can host elevated concentrations of platinum-group elements, the Budgell Harbour area is of considerable interest in economic geology [39]. The regional geology of the Budgell Harbour area is shown in Figure 1. Given its expected higher density and magnetic susceptibility relative to the host rocks, the BHS represents an appropriate target for both magnetic and gravity geophysical surveys [26, 44].

From an economic geology standpoint, mafic intrusions of this type may host Fe–Ti–V oxides, Ni–Cu sulfide assemblages, and locally platinum-group element (PGE) mineralization. However, the area's primary significance to date has remained largely academic, with research emphasizing its tectonic evolution and regional geological framework [23]. The BHS is characterized by pronounced topographic relief, and dense forest cover limits accessibility, complicating detailed fieldwork. Moreover, intense weathering has prevented the collection of fresh, unaltered samples necessary for robust geochemical and petrological analyses. As a result, the deeper levels of the intrusion remain poorly exposed and poorly constrained due to both weathering and restricted field access [23, 45]. Figure 2 presents selected images illustrating the geology of this region.

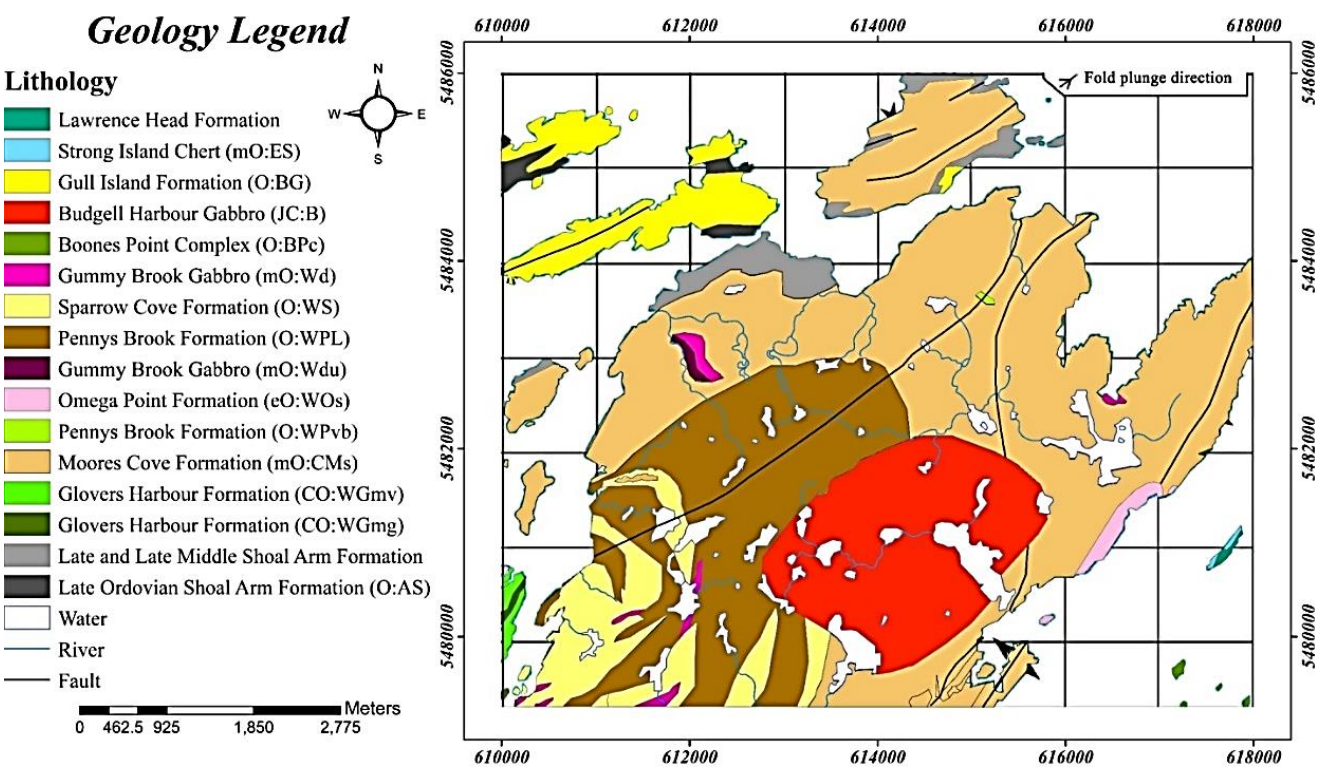

Figure 1. Detailed geological map of the Budgell Harbour Stock (BHS) unit showing the main lithological units, structural features, and the extent of the study area used for geophysical modeling and interpretation [46].

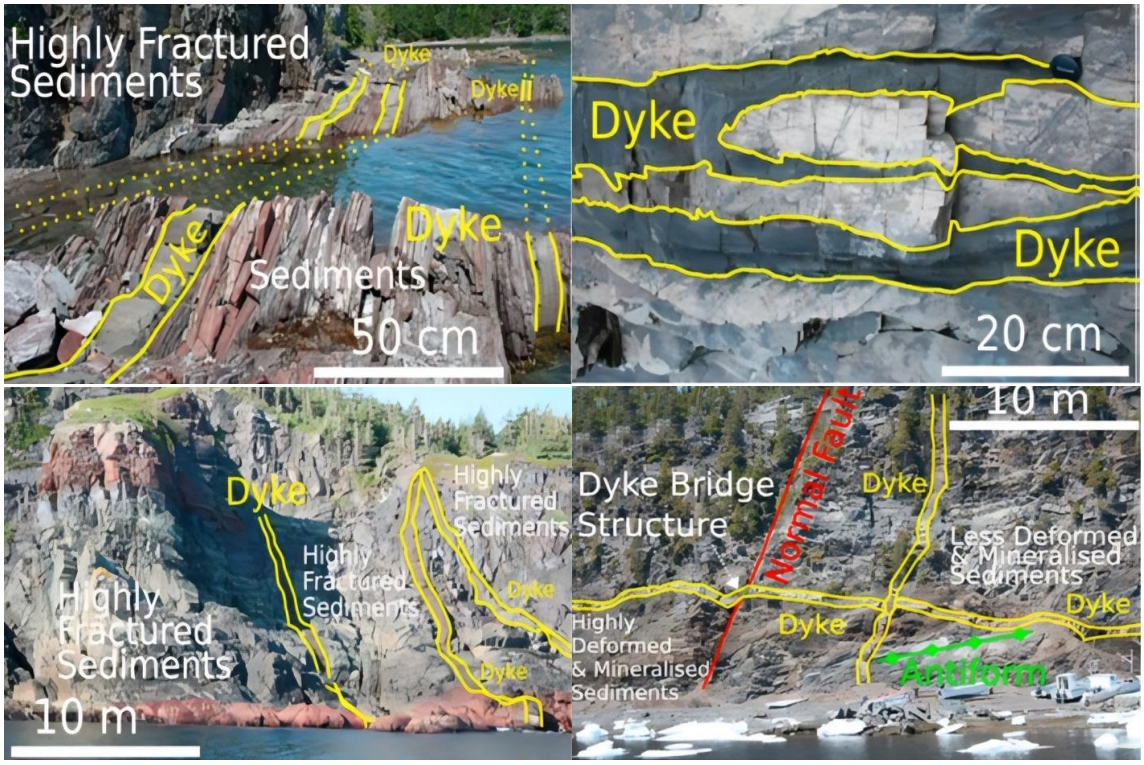

Figure 2. Representative field photographs of outcrops from the Budgell Harbour Stock (BHS) unit, illustrating the main lithological characteristics and surface exposure of the gabbroic intrusion within the study area [23].

4. Airborne geophysics survey

The geophysical data used in this study were collected over the Budgell Harbour Stock in central Newfoundland, within the Notre Dame Bay region. The survey was commissioned by Celtic Minerals Ltd. and carried out in 2007 by Bell Geospace Inc. using the Airborne Full Tensor Gradiometry (Air-FTG®) system. The dataset was later made available by the Geological Survey of Newfoundland and Labrador for research purposes. The FTG survey covers approximately 407 line-km over an area of about 39 km². Flight lines were oriented north–south with a spacing of 200 m, while east–west tie lines were flown at 2000 m intervals. The nominal flight altitude was around 80 m, although terrain-following conditions caused variations ranging from 70 m to 265 m due to topographic relief. The Air-FTG system measures the full gravity gradient tensor, representing the second-order spatial derivatives of the gravitational potential. Among these, the vertical component T_zz was selected for interpretation due to its higher sensitivity to near-surface density variations and its ability to delineate the geometry of the underlying intrusive body. Raw FTG data were processed by Bell Geospace using proprietary workflows, including aircraft motion correction, high-rate post-mission compensation (HRPMC), terrain correction, leveling, and topographic adjustment using an assumed density of 2.70 g/cm³. All tensor components are expressed in Eötvös units (1 E = 0.1 mGal/km).

Complementary airborne magnetic data were also incorporated to enhance subsurface interpretation. These data were acquired using a cesium vapor magnetometer mounted in a stinger configuration and were obtained from the Geological Survey of Canada GEOSCAN database. The TMI data were corrected for diurnal variations, removed for the IGRF reference field, and leveled to produce residual magnetic anomalies. The magnetic survey consisted of flight lines spaced at approximately 1000 m with a mean flight altitude of 120 m. A pronounced dipolar anomaly was observed over the study area, indicating a single dominant magnetic source with an estimated diameter of approximately 4 km. The integration of FTG and magnetic datasets provide complementary sensitivity to subsurface physical properties: FTG data primarily constrain density variations, whereas magnetic data reflect variations in magnetic susceptibility associated with mafic–ultramafic mineralogy. This joint interpretation significantly reduces ambiguity in subsurface modelling and improves the resolution of lithological and structural boundaries within the BHS.

All data were referenced to the WGS-84 coordinate system and projected in UTM Zone 21N, which fully covers the study area located in central Newfoundland. Quality control procedures included removal of line-to-line discrepancies and filtering of high-frequency noise prior to inversion.

5. Synthetic scenarios

This section introduces a synthetic model intended to assess the performance of the inversion methods in reconstructing gravity and magnetic anomalies attributable to a subsurface structure. The model simulates a homogeneous body with a prescribed physical property contrast under controlled conditions, thereby providing a reference for evaluating the behavior and resolution capacity of the inversion algorithm. The synthetic model consists of a three-dimensional subsurface body spanning depths from 800 m to 6000 m. Laterally, the body is bounded between 5000 m and 7000 m in both the east–west and north–south directions, producing a resolvable target in potential-field data. The geometry is deliberately selected as a simple block-shaped body to ensure that the evaluation primarily focuses on the inversion method's ability to recover physical property distributions, rather than on accommodating geometric complexity. In terms of physical properties, the body was assigned a density contrast of 0.6 g/cm³ in the gravity model and a magnetic susceptibility of 0.3 SI in the magnetic model. In both cases, the surrounding host rock was assumed to be homogeneous, with no significant physical-property contrast. This combination of parameters allows the simultaneous generation of

gravity and magnetic responses from a single structure representative of the gabbroic body under investigation in Newfoundland. To simulate realistic survey conditions, the synthetic data were contaminated with random Gaussian noise. Specifically, Gaussian noise equivalent to 1% of the signal amplitude was added to the gravity data, and 2% noise was added to the magnetic data. The resulting observed data are presented in Figure 3, where the tensor gravity response (g_{zz}) and total magnetic field are shown together with sections of the density and magnetic susceptibility models along the Easting and Northing directions.

To simulate realistic geophysical survey conditions, a flat topography was assumed across the entire modeling area. This assumption removes additional effects associated with surface-relief variations and allows the analysis to focus exclusively on the response generated by the subsurface body. Moreover, the resulting synthetic data provide an appropriate basis for evaluating the intrinsic performance of the inversion procedure without the influence of near-surface geometric effects. The gravity and magnetic data were simulated using a uniform acquisition grid at the ground surface to ensure adequate coverage of the target area. The dimensions of the discretized model mesh were $60 \times 60 \times 100$. Next, individual inversion of both gravity and magnetic data was performed using different combinations of ℓ_{pq} norms to evaluate the effect of the regularization type on the quality of model reconstruction. The inversion results for the two-dimensional sections along different directions are presented in Figs. 4 and 5. In these plots, the left column corresponds to the density model, while the right column represents the magnetic susceptibility model. The different rows show the inversion results for the [2,2,2,2], [1,1,1,1], and [0,0,0,0] norm combinations (p_s, q_x, q_y, q_z), respectively, where variations in the smallness term directly control the degree of blockiness or smoothness in the recovered models. All other parameters were kept constant, and only the regularization terms were varied. For all models, the maximum number of iterations was set to 30 to ensure a consistent stopping criterion across all cases. These sections were extracted along Easting = 6 km (Figure 4) and Northing = 6 km (Figure 5), respectively.

A quantitative evaluation of inversion quality was conducted by analyzing the predicted data and their respective misfits relative to the observed data. Figure 6 presents the gravity data results and associated misfits, wherein the left column shows the predicted data derived from the inversion and the right column illustrates the corresponding misfits. The magnetic data results and their misfits are similarly displayed in Figure 7. In both figures, the rows sequentially represent the [2,2,2,2], [1,1,1,1], and [0,0,0,0] norm combinations.

The final RMS data misfit values obtained for the gravity inversion are 8.07%, 8.95%, and 8.85% for the ℓ_0, ℓ_1 and ℓ_2 norm formulations, respectively. For the magnetic data, the corresponding RMS values are 15.67%, 15.84%, and 14.26%, respectively. Collectively, these results demonstrate that the regularization type exerts a direct control on the structural attributes of the inverted model. Sparsity-promoting norm combinations (e.g., [0,0,0,0]) are more proficient at recovering sharp boundaries and concentrating anomalous features, whereas smoother norms (e.g., [2,2,2,2]) produce more continuous models but with less distinct interfaces

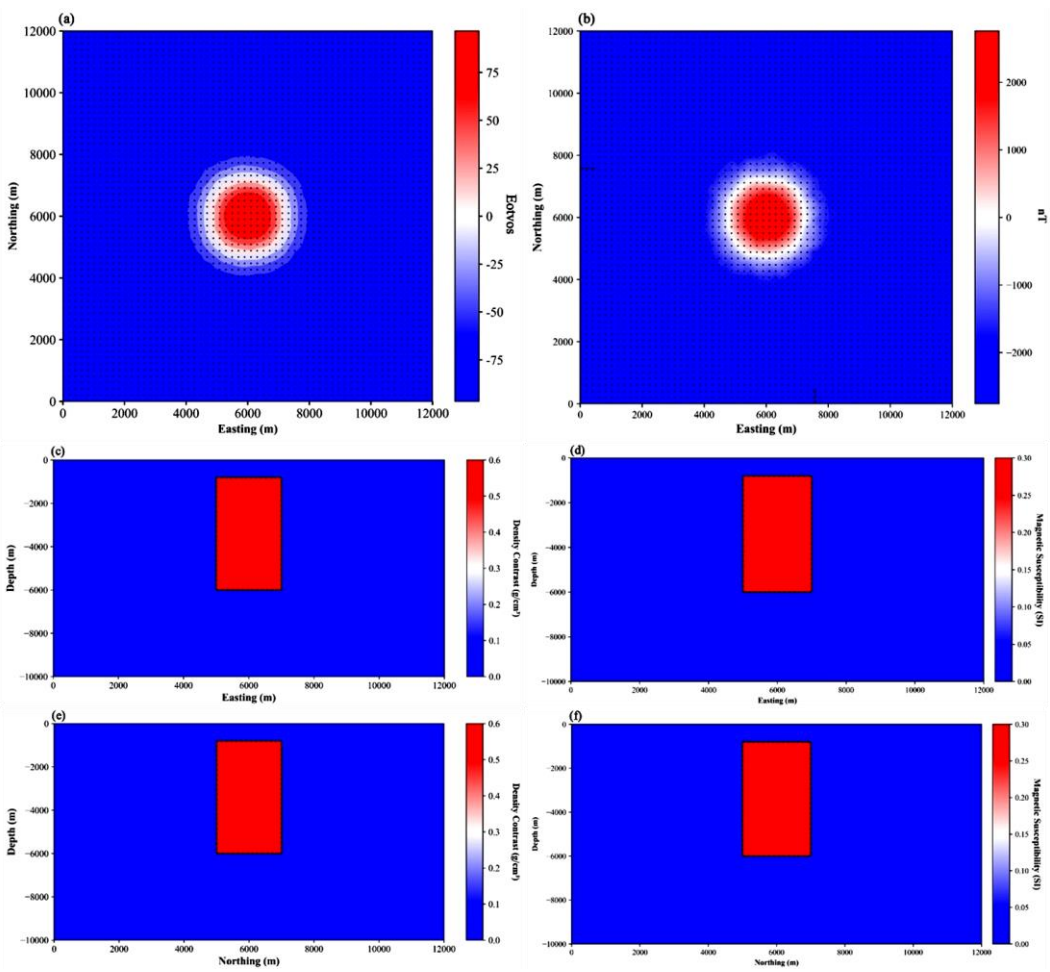

Figure 3. Left column shows the synthetic gravity data and the right one is for total field magnetic data. Top row shows observed g_zz gravity data (a), and total field magnetic data (b). The middle row shows the density contrast model (c) and the magnetic susceptibility model (d) at Northing=6km. The bottom row shows the density contrast model (e) and the magnetic susceptibility model (f) at Eating=6 km. Note that gravity and magnetic data were corrupted respectively by the random Gaussian noise equal to 1% and 2% of the data amplitude.

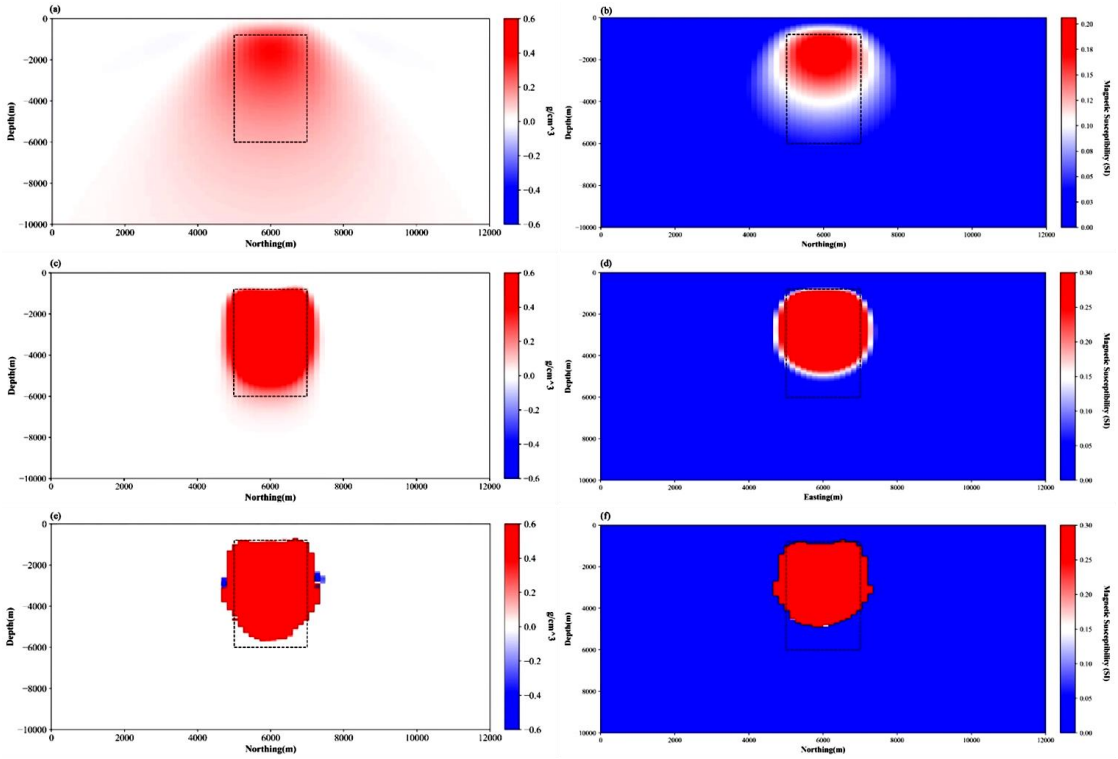

Figure 4. Left column show the inversion results of synthetic gravity data and the right one is for magnetic data. Top row is the inversion result for the density contrast model (a) and magnetic susceptibility model (b) for norm 2222. The middle is the inversion result for the density contrast model (c) and magnetic susceptibility model (d) for norm 1111. The bottom row is the inversion result for the density contrast model (e) and magnetic susceptibility model (f) for norm 0000. The cross sections were extracted at Easting=6 km.

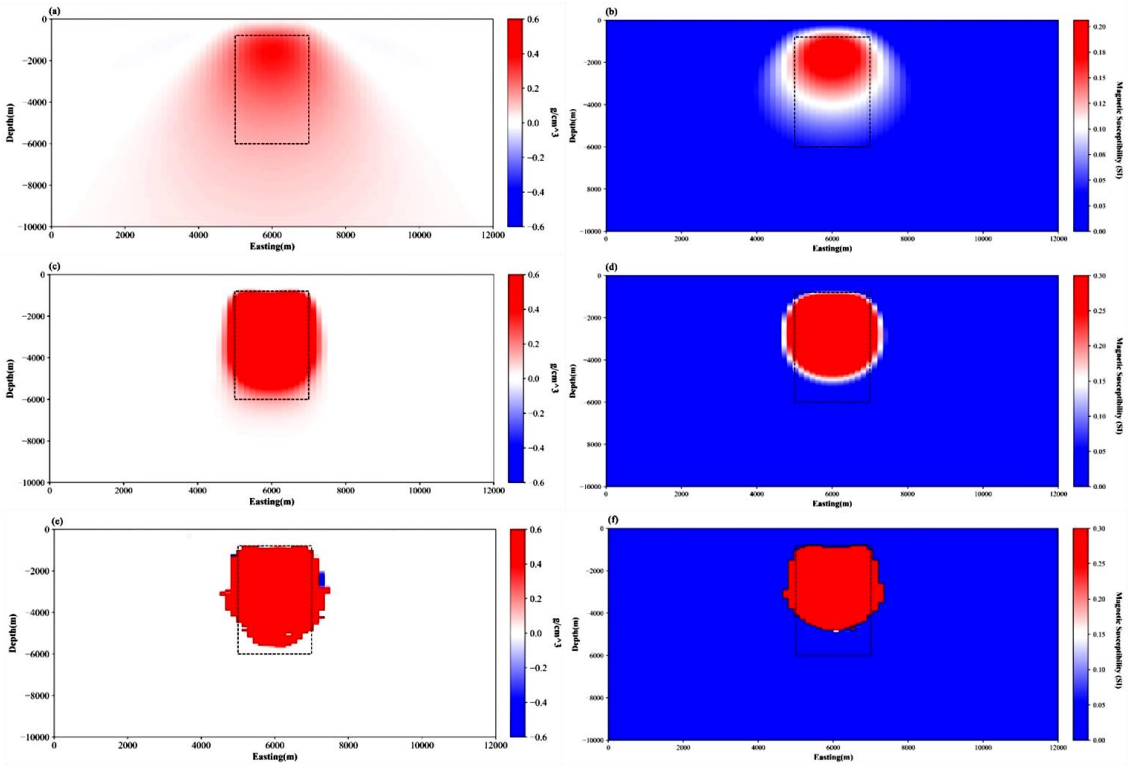

Figure 5. Left column show the inversion results of synthetic gravity data and the right one is for magnetic data. Top row is the inversion result for the density contrast model (a) and magnetic susceptibility model (b) for norm 2222. The middle is the inversion result for the density contrast model (c) and magnetic susceptibility model (d) for norm 1111. The bottom row is the inversion result for the density contrast model (e) and magnetic susceptibility model (f) for norm 0000. The cross sections were extracted at Northing=6 km.

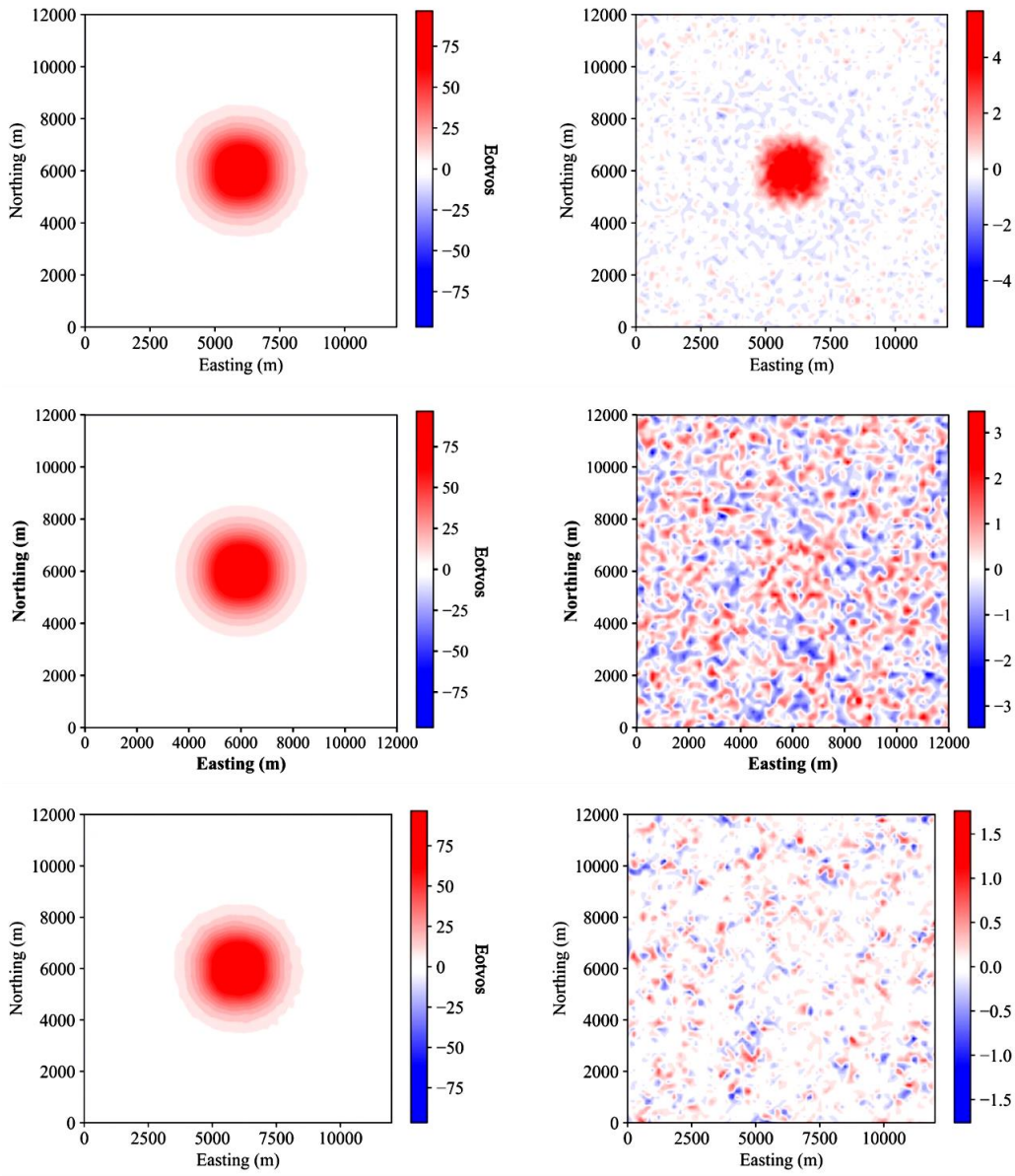

Figure 6. Left column shows the predicted data derived from synthetic tensor gravity data inversion and the right one is the misfit plot. Top row is for norm 2222, the middle row is for norm 1111, and the bottom row is for norm 0000.

Residual and predicted data analyses indicate that both gravity and magnetic datasets are generally well fitted, although their sensitivity to the choice of norm differs. The synthetic model presented herein serves as a baseline for gravity and magnetic inversion, aimed at evaluating the method's capability to recover the location, depth, and physical properties of a single anomaly under different mixed-norm regularization schemes. In particular, the model enables an assessment of the sensitivity of both geophysical methods to density and magnetic susceptibility contrasts, offering a robust framework for comparing inversion results across two independents yet physically coupled domains.

6. Inversion results

Inversion of gravity and magnetic data from a gabbroic body in Newfoundland was carried out to evaluate the performance of different regularization methods in subsurface structure reconstruction. Data uncertainty was assigned as a constant floor value corresponding to 2% of the maximum residual anomaly for each dataset—2% of the gravity residual maximum and 2% of the magnetic residual maximum. For the gravity inversion, the allowable density contrast bounds were set between −0.6 and +0.6 g/cm³, whereas for the magnetic inversion, the magnetic susceptibility bounds were defined between 0 and 0.3 SI. These constraints were imposed to inhibit model divergence and to preserve the physical consistency of the results. The inversion procedure for both gravity and magnetic datasets was conducted independently under three regularization regimes, specifically the [0,0,0,0], [1,1,1,1], and [2,2,2,2] norm configurations, thereby enabling a systematic evaluation of the effects of sparsity and smoothness on the recovered models.

These three cases yield progressively smoother model characteristics, corresponding to blocky, intermediate, and smooth structural outcomes, respectively. The observed data and inversion results along various profiles are displayed in Figs. 8–10. As shown in Figure 8, the primary gravity and magnetic anomalies associated with the gabbroic body are spatially coincident and clearly discernible, though notable differences in their lateral extent and amplitude are evident.

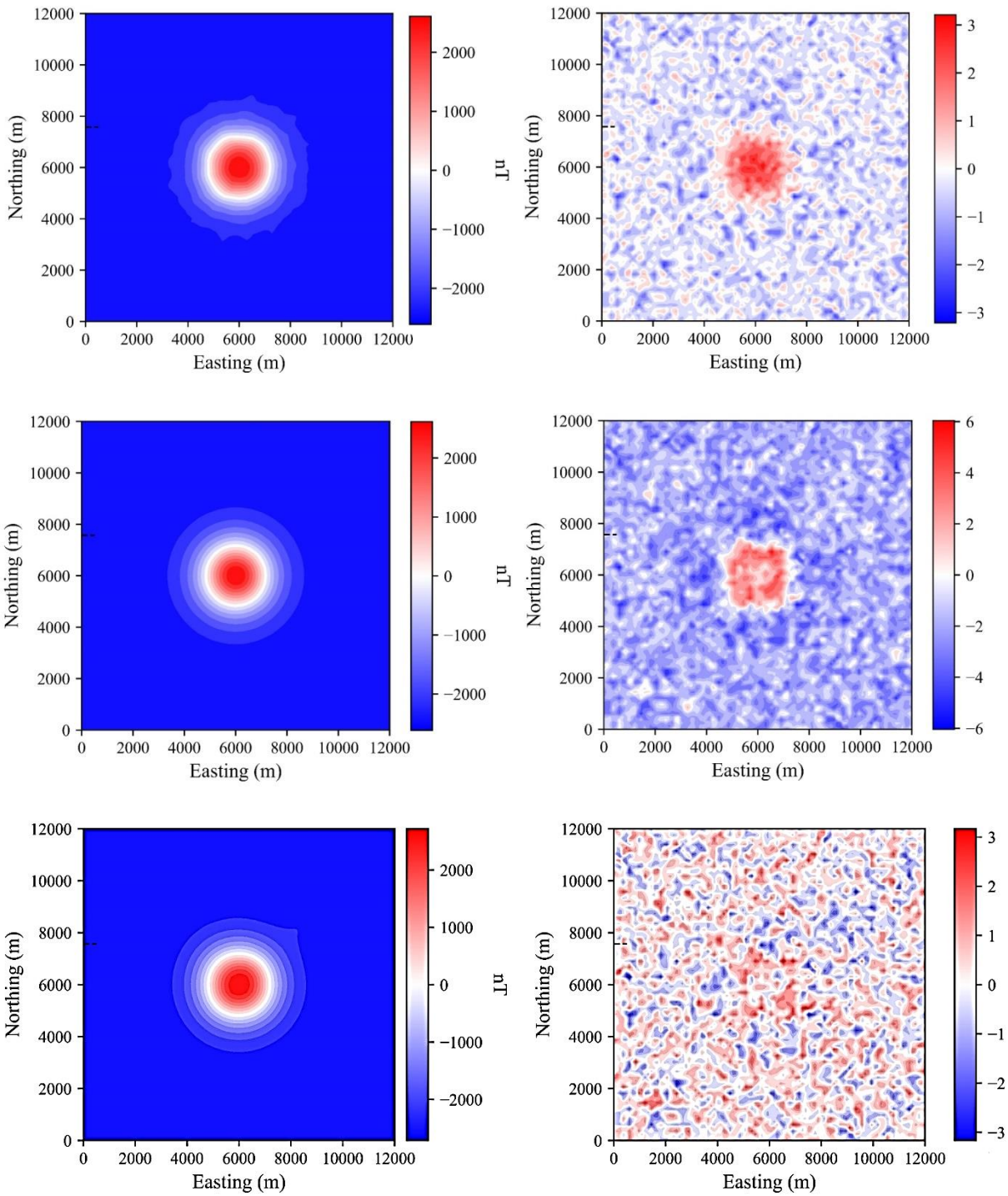

Figure 7. Left column shows the predicted data derived from synthetic total field magnetic data inversion and the right one is the misfit plot. Top row is for norm 2222, the middle row is for norm 1111, and the bottom row is for norm 0000.

As illustrated in Figure 9, the gravity inversion results demonstrate that, under the [0,0,0,0] norm configuration, the recovered model is characterized by sharp boundaries and a highly concentrated anomaly in the central region, resulting in a compact and clearly delineated reconstruction of the gabbroic body. Conversely, the [2,2,2,2] norm configuration produces a smoother model in which the lateral boundaries of the body are progressively smeared, giving rise to an apparent increase in the anomaly's horizontal extent. The [1,1,1,1] norm case represents an intermediate behavior, effectively retaining structural information while faithfully reproducing the general trend of density contrasts.

A similar pattern is observed in the magnetic inversion results (Figure 10); nevertheless, magnetic susceptibility exhibits greater sensitivity to structural boundaries and provides a more distinct delineation of the gabbroic core. The [0,0,0,0] norm model achieves the highest boundary resolution, whereas the [2,2,2,2] norm model places greater emphasis

on regional trends and background variations. This behavior underscores the critical role of regularization in controlling the degree of focusing or smoothing in the magnetic response.

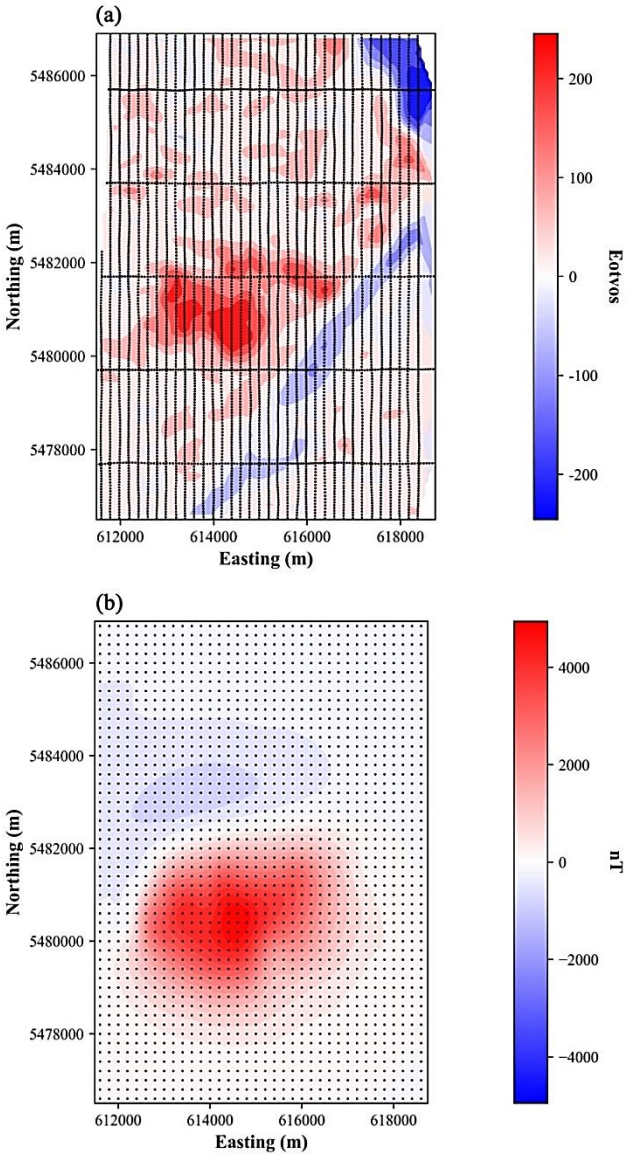

Figure 8. Observed tensor gravity component g_zz (a) and total field magnetic data (b) over the BHS unit.

Comparison of the predicted data with the corresponding misfit distributions (Figures 11 and 12) reveals that all three regularization settings successfully reconstruct the general anomaly pattern. Nevertheless, the primary distinctions lie in the amplitude of localized errors and the spatial character of the residuals. Under sparser norm configurations, the misfit is largely confined to regions adjacent to model boundaries. In contrast, smoother norm configurations produce residuals that are more spatially dispersed yet of lower overall magnitude.

The final RMS data misfit values obtained for the gravity inversion are 10.61%, 10.24%, and 9.74% for the l_0, l_1 and l_2 norm formulations, respectively. For the magnetic data, the corresponding RMS values are 9.56%, 9.43%, and 8.31%, respectively.

In summary, the findings reveal that inversion strategies based on sparser norm formulations (particularly the [0,0,0,0] case) possess enhanced capability to recover sharp lithological boundaries and the compact morphology of the gabbroic body. Conversely, higher-order norms produce more stable model reconstructions but at the cost of reduced boundary definition. This contrast is most conspicuous in the magnetic data, which exhibit greater sensitivity to lithological variations. The mutual consistency between gravity and magnetic inversion results indicates that the Newfoundland gabbroic body presents as a spatially coincident anomaly, although its expression differs across the two geophysical domains. This consistency underscores that the joint application of multiphysics data, coupled with judicious regularization selection, significantly improves interpretive confidence in complex subsurface environments.

7. Discussion

In this section, the results obtained from the inversion of both synthetic and real datasets are discussed within the framework of different regularization schemes to evaluate the physical and numerical behavior of the methods under varying geological conditions. The primary focus is on assessing the performance of mixed-norm approaches in reconstructing subsurface structures with different geometries and mineralization characteristics. Overall, the results indicate that no single regularization strategy can be considered universally optimal; rather, the performance of each method is strongly dependent on the geological setting and the characteristics of the exploration target. In the synthetic models, which consist of bodies with well-defined boundaries and controlled geometries, sparse methods (ℓ_0 and ℓ_1 norms) are capable of reconstructing sharp interfaces and compact anomalies with higher resolution. In contrast, the Tikhonov approach (ℓ_2 norm) produces smoother models that, although effective in recovering the general structural trends, shows limitations in accurately resolving boundaries and distinguishing discrete bodies.

However, this apparent superiority of sparse methods should be interpreted with caution, as synthetic models are inherently biased toward edge-preserving reconstructions. As demonstrated by the results, both approaches were implemented under identical inversion and discretization conditions, and the observed differences arise primarily from the nature of the regularization rather than from variations in the data or computational parameters. Therefore, the comparison mainly reflects the relative behavior of regularization schemes in response to idealized structures, rather than their absolute performance. In the real data from the Newfoundland gabbroic body, geological complexity plays a significant role in moderating the behavior of these regularization approaches. The results indicate that gravity and magnetic responses in this environment act in a complementary manner, each providing distinct information about the subsurface structure. Gravity data are primarily sensitive to density variations associated with mafic and gabbroic bodies, whereas magnetic data are more effective in delineating zones related to magnetic mineralization and variations in mineralogical composition. In this context, sparse regularization is capable of reconstructing compact, high-contrast regions with greater spatial focusing, particularly in resolving gabbroic cores and zones with strong magnetic responses. In contrast, Tikhonov regularization produces more continuous and spatially extensive structures, which are better suited for interpreting regional trends and gradual variations in density and magnetic susceptibility. This difference can be directly attributed to the mathematical nature of these regularization schemes, where (ℓ_2) tends to distribute model energy more diffusely, whereas (ℓ_0/ℓ_1)-based approaches promote spatial concentration of the model.

An important observation from the real data is that, unlike the synthetic models, both approaches ultimately yield relatively consistent models in terms of the overall location of the anomalies. This suggests that, in natural systems, the presence of noise, geological heterogeneity, and structural uncertainties reduces excessive sensitivity to the choice of regularization, allowing both approaches to provide a reasonable first-order representation of the subsurface. Although the ℓ_0, ℓ_1 and ℓ_2 regularization schemes lead to slightly different misfit levels, all three approaches produce consistent inversion results with comparable data

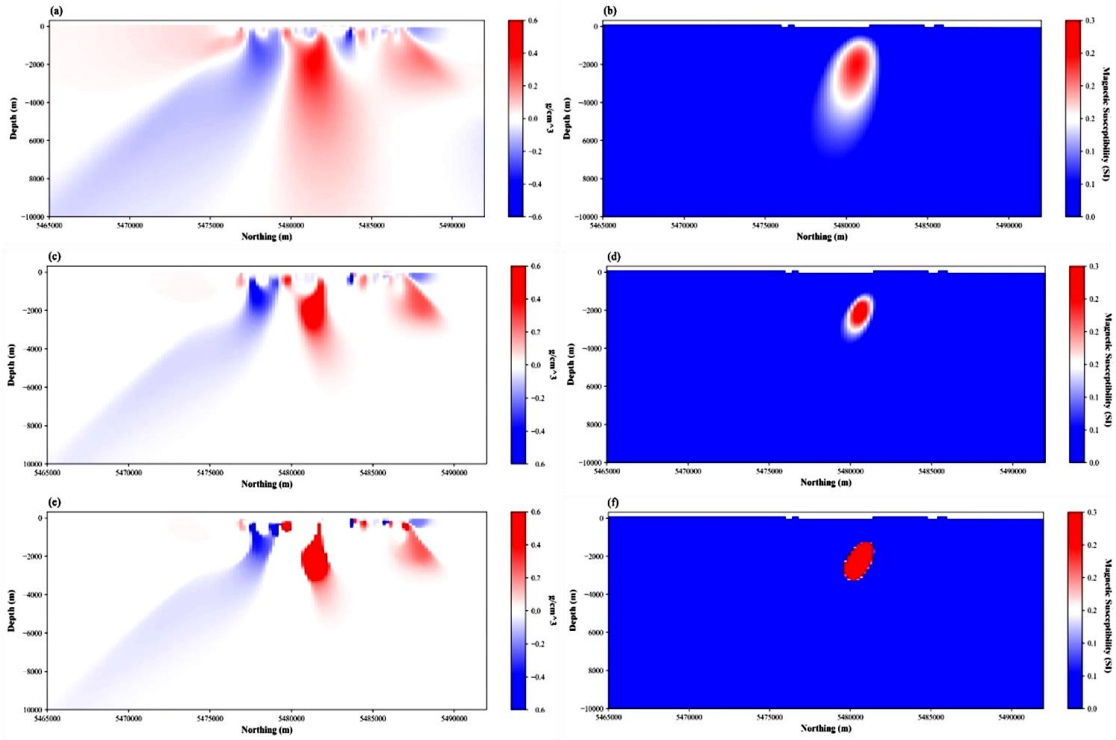

Figure 9. Left column show the inversion results of the tensor gravity data and the right one is for the magnetic data over the BHS unit. Top row is the inversion result for the density contrast model (a) and magnetic susceptibility model (b) for norm 2222. The middle is the inversion result for the density contrast model (c) and magnetic susceptibility model (d) for norm 1111. The bottom row is the inversion result for the density contrast model (e) and magnetic susceptibility model (f) for norm 0000. The cross sections were extracted at Easting= 610260 km.

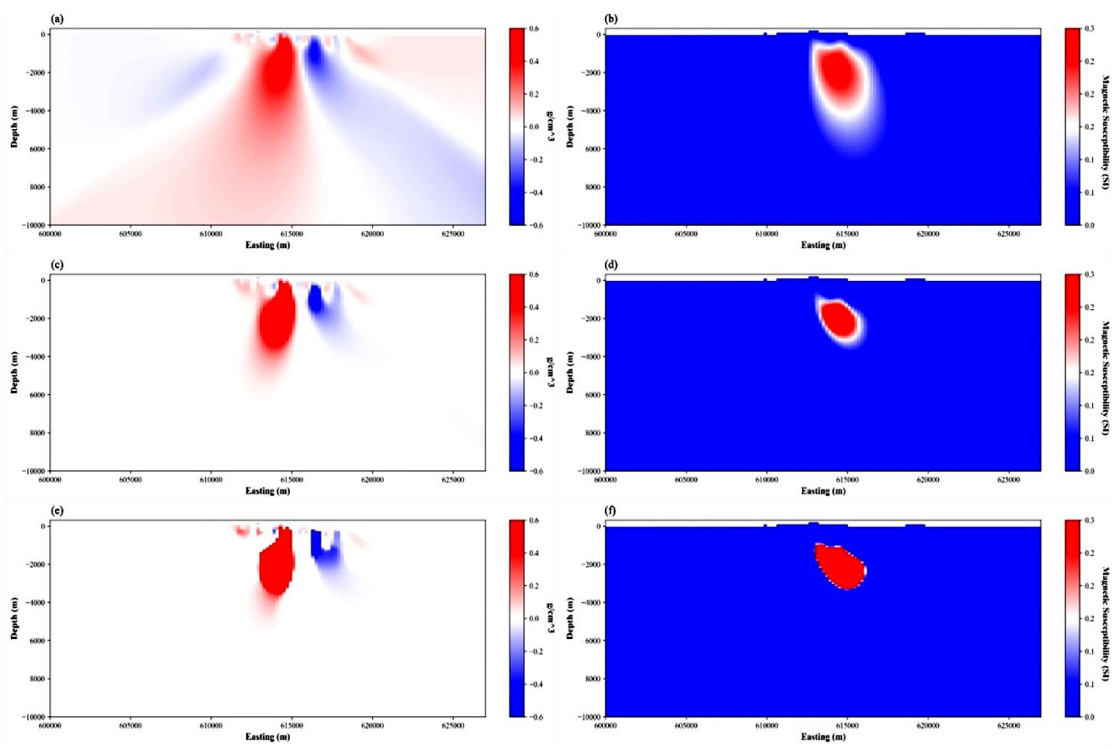

Figure 10. Left column show the inversion results of the tensor gravity data and the right one is for the magnetic data over the BHS unit. Top row is the inversion result for the density contrast model (a) and magnetic susceptibility model (b) for norm 2222. The middle is the inversion result for the density contrast model (c) and magnetic susceptibility model (d) for norm 1111. The bottom row is the inversion result for the density contrast model (e) and magnetic susceptibility model (f) for norm 0000. The cross sections were extracted at Northing= 5475260 km.

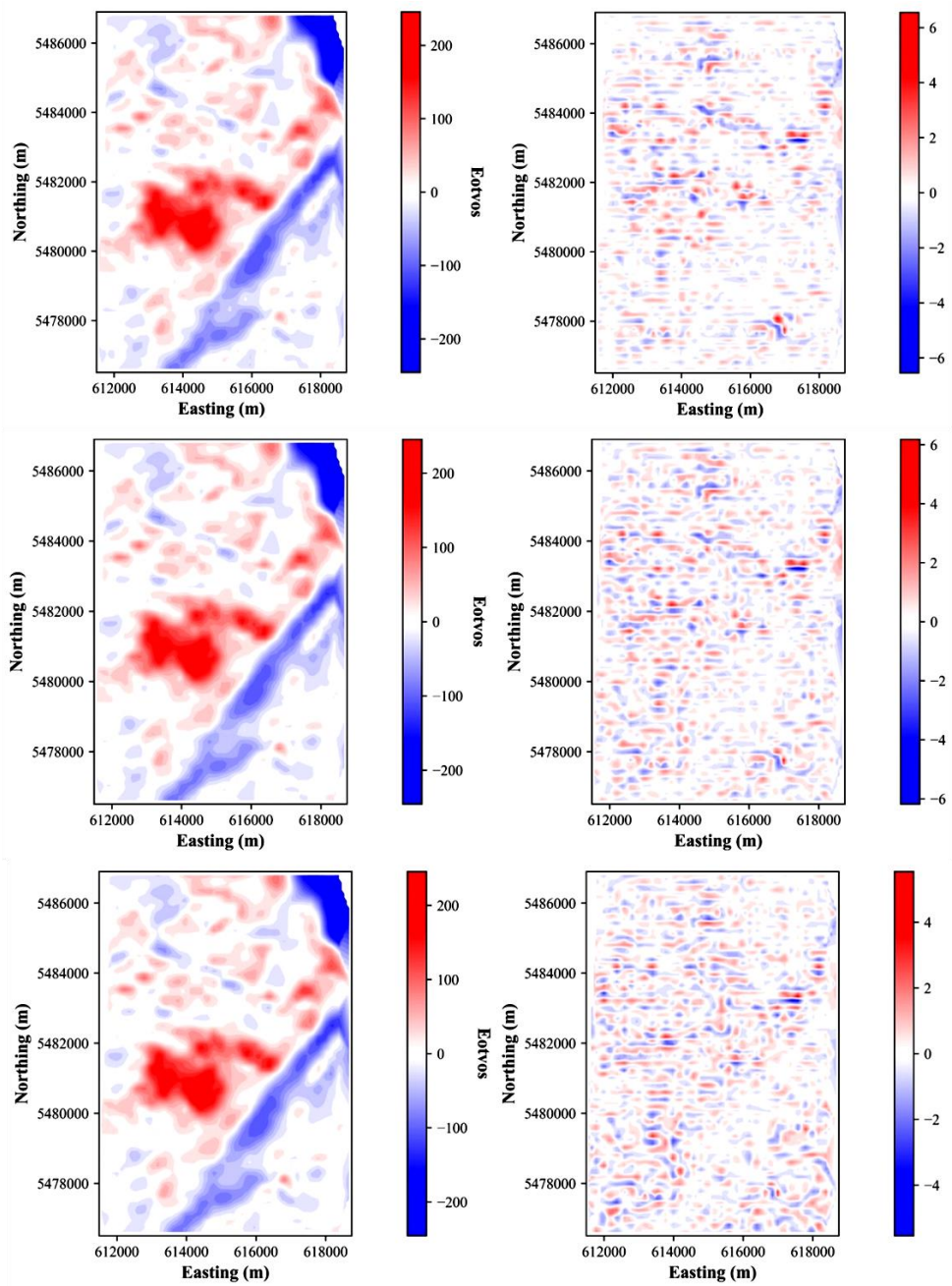

Figure 11. Left column shows the predicted data derived from the tensor gravity inversion over the BHS unit and the right one is the misfit plot. Top row is for norm 2222, the middle row is for norm 1111, and the bottom row is for norm 0000.

fitting performance. The observed differences are primarily associated with the varying sparsity and smoothness constraints imposed by each norm. It is important to note that the final misfit values do not reach the assumed noise levels. This behavior is expected in strongly regularized geophysical inverse problems, where the solution is governed by a balance between data fidelity and model regularization rather than strict data fitting. In such frameworks, enforcing convergence to the noise level may lead to overfitting and loss of geological plausibility. Therefore, the inversion is terminated based on a combination of misfit reduction, model stability, and convergence behavior, ensuring robust and geologically meaningful models. From a geological interpretation perspective, the consistency between gravity and magnetic results in identifying the Newfoundland gabbroic core confirms that this body manifests as a multiphysics anomaly, with each physical field responding differently to its various components. This highlights the importance of integrating multiple geophysical datasets, as reliance on a single dataset may lead to incomplete or biased interpretations of subsurface structures. Ultimately, the results of this study demonstrate that the choice between sparse and smooth regularization should not be made in an absolute sense, but rather should depend on the exploration objective, deposit type, and the scale of geological variability. In systems characterized by sharp boundaries and highly concentrated mineralization, sparse regularization offers clear advantages, whereas in more complex environments with gradual variations, Tikhonov regularization provides a more stable and reliable representation. A judicious combination of these approaches can provide an optimal framework for reducing uncertainty and enhancing the interpretability of inversion models in geophysical exploration.

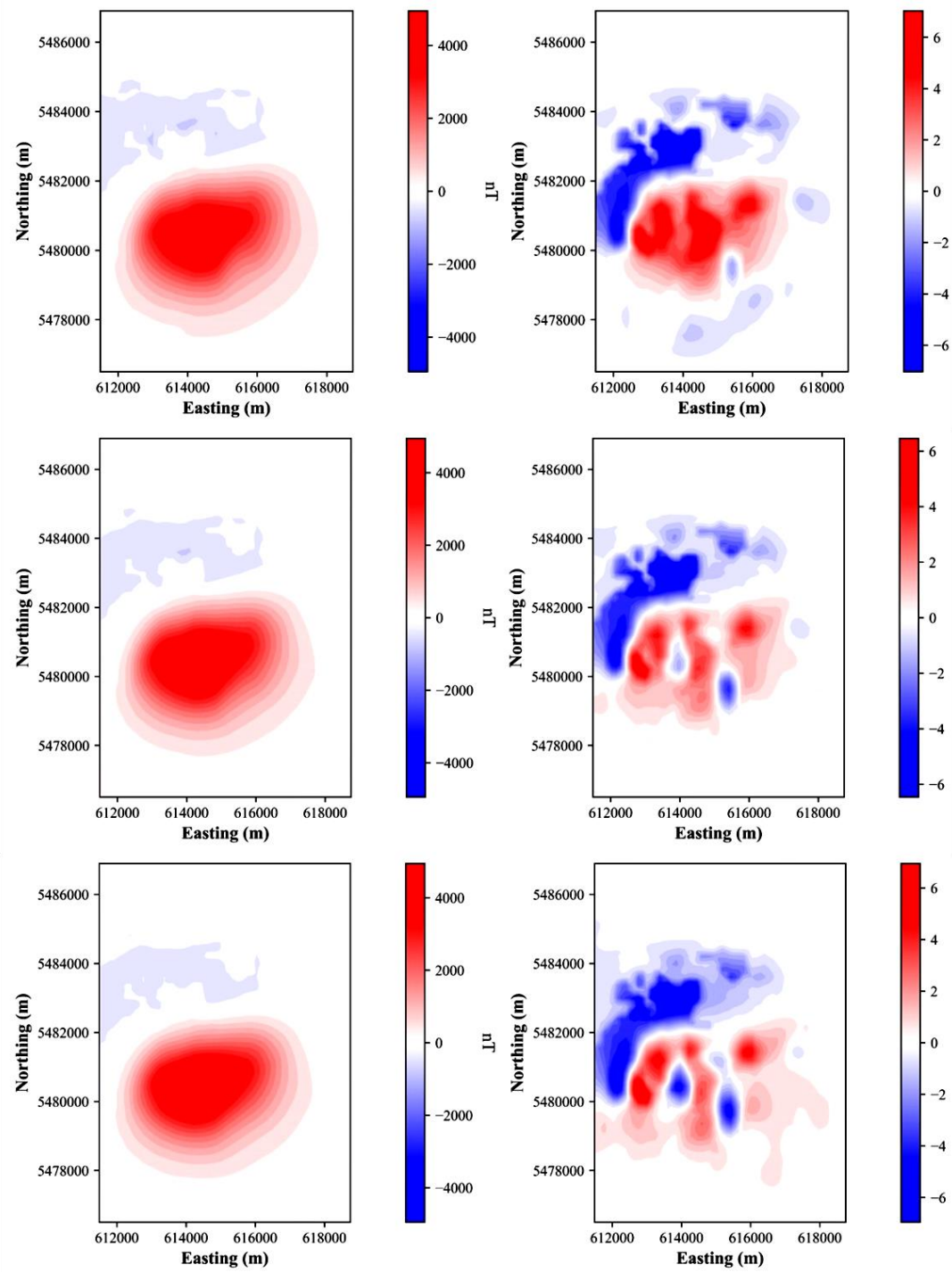

Figure 12. Left column shows the predicted data derived from the magnetic inversion over the BHS unit and the right one is the misfit plot. Top row is for norm 2222, the middle row is for norm 1111, and the bottom row is for norm 0000.

8. Conclusions

In this study, inversion of geophysical data, including the tensor gravity component and total magnetic intensity data associated with the Newfoundland gabbroic body, was performed using a mixed-norm regularization framework. The main objective was to investigate the effect of different norm choices (p or $q = 0, 1$ and 2) on the quality of subsurface reconstruction and to evaluate the capability of each setting in resolving geological anomalies. The results demonstrate that the choice of regularization has a decisive influence on the nature of the inverted models. Smaller norms (particularly the l_0 case) produce more compact models with sharp boundaries and higher anomaly concentration, making them more suitable for identifying dense cores and magnetized zones within the gabbroic body. In contrast, larger norms (notablyl_2) yield smoother and more laterally extensive models that, while effective in capturing regional trends and large-scale

structures, exhibit a reduced ability to precisely delineate geological boundaries. The intermediate case (l_1) provides a balance between these two extremes, achieving a compromise between structural resolution and model stability.

A comparison of the gravity and magnetic results indicates that both datasets are capable of identifying the overall gabbroic body; however, their differing sensitivities to physical properties lead to complementary responses. Gravity data are more sensitive to density variations associated with the gabbroic body and play a more important role in reconstructing the overall geometry and approximate depth of the structure, whereas magnetic data are more effective in delineating magnetized zones and revealing internal structural details. Overall, the results of this study demonstrate that none of the tested norms is universally superior, and their performance depends on the nature of the geological target. In systems characterized by sharp boundaries and concentrated anomalies, more sparse regularization (close to l_0) is more appropriate, whereas for reconstructing continuous trends and broader structures, higher-order norms provide more stable and reliable results. Finally, the use of a multi-norm regularization framework helps reduce uncertainty and increases modeling flexibility, indicating that a judicious combination of these settings can serve as an effective tool for more accurate interpretation of multiphysics geophysical data in mineral exploration studies.

Acknowledgements

The authors wish to express their heartfelt gratitude to the School of Mining Engineering at the University of Tehran for their invaluable support.

References

[1]. Best, M. G. (2002). Igneous and metamorphic petrology. John Wiley & Sons.

[2]. Kearey, P., Brooks, M., & Hill, I. (2002). An introduction to geophysical exploration (Vol. 4). John Wiley & Sons.

[3]. Philpotts, A. R., & Ague, J. J. (2009). Principles of igneous and metamorphic petrology. Cambridge University Press.

[4]. Fowler, C. M. R. (1990). The solid earth: An introduction to global geophysics. Cambridge University Press.

[5]. Singh, B., et al. (2014). Combined gravity and magnetic modeling over Pavagadh and Phenaimata igneous complexes, Gujarat, India: Inference on emplacement history of Deccan volcanism. Journal of Asian Earth Sciences, 80, 119–133. doi: https://doi.org/10.1016/j.jseaes.2013.11.005

[6]. Rey-Moral, C., et al. (2022). Recording the largest gabbro-anorthositic complex worldwide: The Kunene Complex (KC), SW Angola. Precambrian Research, 379, 106790. doi: https://doi.org/10.1016/j.precamres.2022.106790

[7]. Filatova, V. (2021). Peculiar features of correlation between petrophysical signatures of rocks and distribution of geophysical heterogeneities in the Monchegorsk ore area. Geofizicheskiy Zhurnal, 43(4), 176–198. doi: https://doi.org/10.24028/gzh.v43i4.239969

[8]. Pastore, Z., Fichler, C., & McEnroe, S. A. (2018). Magnetic anomalies of the mafic/ultramafic Seiland Igneous Province. Norwegian Journal of Geology, 98, 79–101. doi: https://doi.org/10.17850/njg98-1-06

[9]. Kamm, J., et al. (2015). Joint inversion of gravity, magnetic, and petrophysical data. Geophysics, 80(5), B131–B152. doi: https://doi.org/10.1190/geo2014-0122.1

[10]. Jordan, T. A., & Riley, T. R. (2024). Reinvestigating the Dufek Intrusion through joint gravity and magnetic models. Physics of the Earth and Planetary Interiors, 356, 107268. doi: https://doi.org/10.1016/j.pepi.2024.107268

[11]. Yang, Y., & Li, Y. (2025). Joint gravity and magnetic modelling for concealed intrusions. Near Surface Geophysics, 23(3), 215–228. doi: https://doi.org/10.1002/nsg.70008

[12]. Abedi, M. (2020). A focused and constrained 2D inversion of potential field data. Physics of the Earth and Planetary Interiors, 309, 106604. doi: https://doi.org/10.1016/j.pepi.2020.106604

[13]. An, S., et al. (2025). Structural analysis of magmatic Ni-Cu sulfide deposit. Ore Geology Reviews, 106916. doi: https://doi.org/10.1016/j.oregeorev.2025.106916

[14]. Bahía, M. E., et al. (2024). Gravity and magnetic surveys for exploration of epithermal project. Journal of South American Earth Sciences, 145, 105049. doi: https://doi.org/10.1016/j.jsames.2024.105049

[15]. Fournier, D. (2019). Advanced potential field data inversion with lp-norm regularization (PhD thesis). University of British Columbia.

[16]. Fournier, D., & Oldenburg, D. W. (2019). Inversion using spatially variable mixed ℓp norms. Geophysical Journal International, 218(1), 268–282. doi: https://doi.org/10.1093/gji/ggz156

[17]. Wei, X., & Sun, J. (2021). Uncertainty analysis of 3D inversion. Geophysics, 86(6), G133–G158. doi: https://doi.org/10.1190/geo2020-0672.1

[18]. Sun, J., & Wei, X. (2021). Recovering sparse models in 3D inversion. Geophysical Prospecting, 69(4), 901–910.

[19]. Chen, T., & Zhang, G. (2022). Mineral exploration potential estimation. Remote Sensing, 14(11), 2537. doi: https://doi.org/10.3390/rs14112537

[20]. Estatico, C., et al. (2017). A conjugate gradient like method for p-norm minimization. Numerische Mathematik, 137(4), 895–922. doi: https://doi.org/10.1007/s00211-017-0893-7

[21]. Fournier, D., Oldenburg, D., & Davis, K. (2016). Robust and flexible mixed-norm inversion. SEG International Exposition and Annual Meeting.

[22]. Wei, X., & Sun, J. (2020). Uncertainty analysis of joint inversion. SEG International Exposition and Annual Meeting.

[23]. Peace, A. L., et al. (2018). Rift-related magmatism on magma-poor margins. Tectonophysics, 745, 24–45. doi: https://doi.org/10.1016/j.tecto.2018.07.025

[24]. Geng, M., et al. (2019). 3D inversion of airborne gradiometry data. Geophysics, 84(4), B269–B284. doi: https://doi.org/10.1190/geo2018-0407.1

[25]. Geng, M., et al. (2018). 3-D inversion of airborne gravity gradiometry data. SEG International Exposition and Annual Meeting.

[26]. Geng, M., et al. (2020). 3-D joint inversion of gravity gradiometry and magnetic data. Geophysical Journal International, 223(1), 301–322. doi: https://doi.org/10.1093/gji/ggaa283

[27]. Geng, M., et al. (2019). 3D joint inversion case study. SEG International Exposition and Annual Meeting.

[28]. Cockett, R., et al. (2015). SimPEG: An open-source framework. Computers & Geosciences, 85, 142–154.

[29]. Zhdanov, M. S. (2015). Inverse theory and applications in geophysics (Vol. 36). Elsevier.

[30]. Nagy, D. (1966). The gravitational attraction of a right rectangular prism. Geophysics, 31(2), 362–371. doi: https://doi.org/10.1190/1.1439779

[31]. Plouff, D. (1976). Gravity and magnetic fields of polygonal prisms. Geophysics, 41(4), 727–741. doi: https://doi.org/10.1190/1.1440645

[32]. Sharma, P. V. (1966). Rapid computation of magnetic anomalies. Pure and Applied Geophysics, 64(1), 89–109. doi: https://doi.org/10.1007/BF00875535

[33]. Li, Y., & Oldenburg, D. W. (1996). 3-D inversion of magnetic data. Geophysics, 61(2), 394–408. doi: https://doi.org/10.1190/1.1443968

[34]. Li, Y., & Oldenburg, D. W. (1998). 3-D inversion of gravity data. Geophysics, 63(1), 109–119. doi: https://doi.org/10.1190/1.1444302

[35]. Oldenburg, D. W., & Li, Y. (2005). Inversion for applied geophysics: A tutorial.

[36]. Ardestani, V. E., Fournier, D., & Oldenburg, D. W. (2022). Localized gravity modeling. Pure and Applied Geophysics, 179(6), 2365–2381.

[37]. Fournier, D., Heagy, L. J., & Oldenburg, D. W. (2020). Sparse magnetic vector inversion. Geophysics, 85(3), J33–J49.

[38]. Cooper, M., et al. (2001). Basin evolution in western Newfoundland. AAPG Bulletin, 85(3), 393–418. doi: https://doi.org/10.1306/8626C901-173B-11D7-8645000102C1865D

[39]. Totoş, O. (2021). 3D modelling and inversion of airborne gravity data (MSc thesis). Memorial University of Newfoundland.

[40]. Castonguay, S., et al. (2009). Structural geology of the Pacquet Harbour group. Geological Survey Report.

[41]. Schofield, D. I., & D'Lemos, R. S. (2000). Granite petrogenesis in Newfoundland. Canadian Journal of Earth Sciences, 37(4), 535–547. doi: https://doi.org/10.1139/e99-116

[42]. Evans, D. T. (1996). Epigenetic gold occurrences. Geological Survey.

[43]. Stuckless, E. (2008). Minerals assessment report. doi: https://doi.org/10.1016/j.dib.2018.10.072

[44]. Miller, H. (1976). A magnetic model for the Budgell Harbour Stock. Canadian Journal of Earth Sciences, 13(2), 231–236. doi: https://doi.org/10.1139/e76-025

[45]. Helwig, J., Aronson, J., & Day, D. (1974). A Late Jurassic mafic pluton. Canadian Journal of Earth Sciences, 11(9), 1314–1319. doi: https://doi.org/10.1139/e74-123

[46]. O'Brien, B. (2006). Geology of the Bay of Exploits—New Bay area (parts of NTS 2E/5, 6, 7, 11), north-central Newfoundland. Scale 1:50,000. Newfoundland and Labrador Department of Natural Resources, Geological Survey, Map 4.